EPJ manuscript No.
(will be inserted by the editor)

Numerical simulation of continuum models for fluid-fluid interface dynamics

Sven Gross[1,a] and Arnold Reusken[1,b]

Institut für Geometrie und Praktische Mathematik, RWTH-Aachen

Abstract. This paper is concerned with numerical methods for two-phase incompressible flows assuming a sharp interface model for interfacial stresses. Standard continuum models for the fluid dynamics in the bulk phases, for mass transport of a solute between the phases and for surfactant transport on the interface are given. We review some recently developed finite element methods for the appropriate discretization of such models, e. g., a pressure XFE space which is suitable to represent the pressure jump, a space-time XFE discretization for the mass transport equation of a solute and a surface finite element method (SurFEM) for surfactant transport. Numerical experiments based on level set interface capturing and adaptive multilevel finite element discretization are presented for rising droplets with a clean interface model and a spherical droplet in a Poisseuille flow with a Boussinesq-Scriven interface model.

1 Introduction

Dynamic properties of interfaces, such as interfacial shear and dilatational viscosities and elasticity, can have a significant effect on the flow behavior. The effects caused by these properties can strongly influence the dynamics of emulsions, of biological fluids, of polymer blends and of many other soft matters. A better understanding of these phenomena is a major topic in the research field of *surface* rheology and in recent years a vast number of papers on dynamic properties of interfaces in soft matters has appeared. We refer to [19] for a recent overview.

Two-phase incompressible flows with interfacial stresses are usually modeled by either a diffusive interface or a sharp interface model. In this paper we restrict to the numerical simulation of the latter class of models. For numerical simulations based on a diffusive interface model we refer to the literature, e.g. [23, 24, 1]. In systems with incompressible fluids a sharp interface model typically consists of the Navier-Stokes equations for the bulk fluids with an interfacial force term on the right-hand side in the momentum equation, cf. Section 4 for more details. This interface force is based on a certain interfacial stress-deformation constitutive law. In this paper, as specific examples we consider a clean interface constitutive law (only surface tension) and the Boussinesq-Scriven viscous interface constitutive law. This fluid dynamics model can

[a] e-mail: gross@igpm.rwth-aachen.de
[b] e-mail: reusken@igpm.rwth-aachen.de

be complemented by continuum models for mass transport (of a solute) and surfactant transport. In this paper we first review these standard continuum models that form the basis for numerical simulations of two-phase incompressible flow problems. We explain why in general these models have a very high numerical complexity. Such flow models can not be solved reliably and accurately by the commercial codes that are available nowadays. There is a need for more efficient numerical techniques for this class of models. In the past decade some new finite element methods for the class of two-phase incompressible flows have been developed. We review some of these, e.g. a finite element technique for discretization of the interfacial forces, an extended finite element method (XFEM) for the accurate approximation of the pressure variable and a space-time finite element technique that is suitable for handling moving discontinuities. We restrict ourselves to an explanation of the main ideas of these methods and refer to the literature for more detailed information. In the last part of the paper we present some results of numerical experiments that were obtained using the DROPS solver [6] that is specifically developed for the simulation of two-phase incompressible flow models. This solver is based on the level set technique for interface capturing and on multilevel finite element discretization methods.

This paper has a review character. Most of the models, methods and numerical experiments presented can be found in recent literature. In this paper we collect these and discuss recent developments, challenges and open problems in the field of numerical simulation of continuum models for fluid-fluid interface dynamics.

2 Continuum models

In this section we summarize standard models, known from the literature, that are based on continuum mechanics and used to describe the behavior of two-phase flow problems, cf., for example [19,22,26,12]. We restrict ourselves to *isothermal conditions*, *incompressible* fluids and assume that there is *no change of phase*. In Section 2.1 we describe the incompressible Navier-Stokes equations with suitable interface conditions, which are used to model the fluid dynamics in a two-phase flow. In Section 2.2 a convection-diffusion equation that models the transport of a solute from one solvent into the other is given. In Section 2.3 a transport equation on the interface is presented which models the concentration distribution of a surfactant on the interface. We consider the following setting. The given domain $\Omega \subset \mathbb{R}^3$, contains two different immiscible incompressible phases (liquid-liquid or liquid-gas) which may move in time and have different material properties ρ_i (density) and μ_i (viscosity), $i = 1, 2$. The density and viscosity, ρ_i and $\mu_i, i = 1, 2$, are assumed to be constant in each phase. For each point in time, $t \in [0, T]$, Ω is partitioned into two open bounded subdomains $\Omega_1(t)$ and $\Omega_2(t)$, $\overline{\Omega} = \overline{\Omega}_1(t) \cup \overline{\Omega}_2(t)$, $\Omega_1(t) \cap \Omega_2(t) = \emptyset$, each of them containing one of the phases. These phases are separated from each other by the interface $\Gamma(t) = \overline{\Omega}_1(t) \cap \overline{\Omega}_2(t)$. For convenience we assume that $\Omega_1(t)$ is strictly contained in Ω, i. e., does not touch $\partial\Omega$.

2.1 Fluid dynamics

The fluid dynamics is modeled by the incompressible Navier-Stokes equations combined with suitable coupling conditions at the interface which describe the effect of interfacial forces. We introduce the normal velocity $V_\Gamma = V_\Gamma(x, t) \in \mathbb{R}$ which denotes the magnitude of the velocity of the interface Γ at $x \in \Gamma(t)$ in normal direction. $\mathbf{n}_\Gamma$ denotes the unit normal on Γ pointing from Ω_1 to Ω_2, often we write $\mathbf{n}$ instead of $\mathbf{n}_\Gamma$. To model interfacial forces we use the following standard (Cauchy) ansatz. The

interface is considered to be a 2D continuum and on each (small) connected surface segment $\gamma \subset \Gamma$, cf. Fig. 1, there is a contact force on $\partial\gamma$ of the form $\boldsymbol{\sigma}_\Gamma n$. This $\boldsymbol{\sigma}_\Gamma$ is called the *interface stress tensor* and constitutive laws for $\boldsymbol{\sigma}_\Gamma$ have to be provided by surface rheology. Examples will be given below.

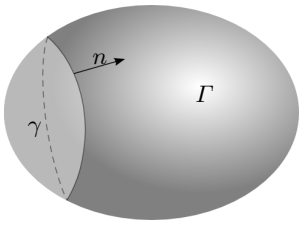

Fig. 1. Interface Γ and subset $\gamma \subset \Gamma$, with vector n which is normal to $\partial\gamma$ and tangential to Γ.

Based on the basic conservation laws of mass and momentum the following standard model (in strong formulation) for the *fluid dynamics* of a two-phase incompressible flow can be derived:

$$\begin{cases} \rho_i(\frac{\partial \mathbf{u}}{\partial t} + (\mathbf{u}\cdot\nabla)\mathbf{u}) & = \operatorname{div}\boldsymbol{\sigma}_i + \rho_i \mathbf{g} \\ \operatorname{div}\mathbf{u} & = 0 \end{cases} \qquad \text{in } \Omega_i, \quad i = 1,2, \tag{1}$$

$$[\boldsymbol{\sigma}\mathbf{n}_\Gamma]_\Gamma = \operatorname{div}_\Gamma \boldsymbol{\sigma}_\Gamma \quad \text{on } \Gamma, \tag{2}$$

$$[\mathbf{u}]_\Gamma = 0 \quad \text{on } \Gamma, \tag{3}$$

$$V_\Gamma = \mathbf{u}\cdot\mathbf{n}_\Gamma \quad \text{on } \Gamma. \tag{4}$$

with the stress tensor $\boldsymbol{\sigma}_i = -p\mathbf{I} + \mu_i\big(\nabla\mathbf{u} + (\nabla\mathbf{u})^T\big)$, i. e., we consider Newtonian bulk fluids. The vector $\mathbf{g}$ denotes an external (gravity) force. The operator $\operatorname{div}_\Gamma$ denotes the tangential divergence, cf. [12]. The notation $[\cdot]_\Gamma$ is used to denote the jump of a quantity across Γ. The assumption that there is no change of phase leads to the dynamic interface condition (4). Viscosity of the fluids leads to the continuity condition in (3). Momentum conservation in a (small) material volume that intersects the interface leads to the stress balance condition in (2). To make the problem well-posed one needs suitable initial conditions for $\Gamma(0)$ and $\mathbf{u}(x,0)$ and boundary conditions for $\mathbf{u}$ or $\boldsymbol{\sigma}\mathbf{n}$ on $\partial\Omega$.

These Navier-Stokes equations model the fluid dynamics. Note that the evolution of the interface $\Gamma(t)$ is *implicitly* defined by this model.

We mention two concrete examples for the interface stress tensor $\boldsymbol{\sigma}_\Gamma$. For an extensive treatment of constitutive models for the surface stress tensor we refer to [19]. For $x \in \Gamma$ we define the projection $\mathbf{P}(x) = I - \mathbf{n}(x)\mathbf{n}(x)^T$. The operator $\nabla_\Gamma = \mathbf{P}\nabla$ is the tangential gradient. In analogy with the approach for a Newtonian bulk fluid the interface stress tensor is assumed to consist of a pressure and a viscous stress:

$$\boldsymbol{\sigma}_\Gamma = \tau\mathbf{P} + L(\mathbf{D}_\Gamma(\mathbf{u})), \quad \mathbf{D}_\Gamma(\mathbf{u}) := \mathbf{P}\big(\nabla_\Gamma\mathbf{u} + (\nabla_\Gamma\mathbf{u})^T\big)\mathbf{P},$$

with L a linear operator. The parameter τ is the surface tension coefficient. The projection $\mathbf{P}$ is used, since $\boldsymbol{\sigma}_\Gamma n = \mathbf{P}\boldsymbol{\sigma}_\Gamma\mathbf{P}n$ should represent only contact forces that are tangential to the surface. For $L = 0$ this contact force reduces to the *surface tension contact force* and the right-hand side in the force balance (2) takes the form

$$\operatorname{div}_\Gamma \boldsymbol{\sigma}_\Gamma = \operatorname{div}_\Gamma(\tau\mathbf{P}) = \tau \operatorname{div}_\Gamma \mathbf{P} + \nabla_\Gamma\tau = -\tau\kappa\mathbf{n} + \nabla_\Gamma\tau. \tag{5}$$

Here κ is the mean curvature of Γ, i. e., $\kappa(x) = \operatorname{div} \mathbf{n}_\Gamma(x)$ for $x \in \Gamma$. If τ is a constant the second term on the right-hand side in (5) vanishes and we obtain the standard *clean interface* model for the interfacial forces. If τ is not constant, the second term $\nabla_\Gamma \tau$ represents the so-called Marangoni forces, which are tangential to Γ.

Now consider the case $L \neq 0$. Using the same principles (isotropy, independence of the frame of reference) as in the derivation of the standard Newtonian stress tensor it can be shown, cf. [22,3], that the interface stress tensor $\boldsymbol{\sigma}_\Gamma$ must have the following form:

$$\boldsymbol{\sigma}_\Gamma = \tau \mathbf{P} + \tilde{\lambda}_\Gamma \operatorname{div}_\Gamma \mathbf{u}\, \mathbf{P} + \mu_\Gamma \mathbf{D}_\Gamma(\mathbf{u}), \tag{6}$$

with parameters $\tilde{\lambda}_\Gamma$, μ_Γ. This is the interface analogon of the bulk stress tensor representation $\boldsymbol{\sigma} = -p\mathbf{I} + \lambda \operatorname{div} \mathbf{u}\, \mathbf{I} + \mu\big(\nabla \mathbf{u} + (\nabla \mathbf{u})^T\big)$ for a Newtonian fluid. Note that in general $\operatorname{div}_\Gamma \mathbf{u} \neq 0$, even if $\operatorname{div} \mathbf{u} = 0$ holds. In case of viscous behavior of the interface one takes $\mu_\Gamma > 0$. For certain cases one can derive conditions on the parameter $\tilde{\lambda}_\Gamma$, for example $\tilde{\lambda}_\Gamma > -\mu_\Gamma$ ([22] sect. 4.9.5). Therefore the interface stress tensor is also often written in the form

$$\boldsymbol{\sigma}_\Gamma = \tau \mathbf{P} + (\lambda_\Gamma - \mu_\Gamma) \operatorname{div}_\Gamma \mathbf{u}\, \mathbf{P} + \mu_\Gamma \mathbf{D}_\Gamma(\mathbf{u}), \tag{7}$$

and one assumes $\lambda_\Gamma = \tilde{\lambda}_\Gamma + \mu_\Gamma > 0$. The constitutive law (7) is called the *Boussinesq-Scriven* law. The parameters μ_Γ and λ_Γ, which we assume to be constants, are referred to as the *interface shear viscosity* and *interface dilatational viscosity*, respectively.

The range of validity of the Boussinesq-Scriven law is rather limited. In many systems with complex fluid-fluid interfaces the interfaces have viscoelastic behavior and then more advanced models for $\boldsymbol{\sigma}_\Gamma$ are needed, cf. [19].

2.2 Mass transport

We consider a two-phase flow problem as described above. We assume that one or both phases contain a dissolved species that is transported due to convection and molecular diffusion and does not adhere to the interface. The concentration of this species is denoted by $c(x,t)$. This flow problem can be modeled by the equations (1)-(4) for the flow variables and a convection-diffusion equation for the concentration c. At the interface we need interface conditions for c. The first interface condition comes from mass conservation, which implies flux continuity. The second condition results from a constitutive equation known as Henry's law, which states that the solubility of a gas in a liquid at a particular temperature is proportional to the pressure of that gas above the liquid. In mathematical terms this relation (at constant temperature) can be formulated as $p = k_{\mathrm{H}}\, c$ where p is the partial pressure of the solute in the gas above the solution, c is the concentration of the solute and k_H is known as the Henry's law constant and depends on the solute, the solvent and the temperature. The same solute in different solvents (at the same temperature) corresponds to different Henry constants, reflecting the different solubility properties of the two solvents. From this it can be deduced, that in a two-phase system with a solute, assuming instantaneous local equilibrium at the interface, there is a constant ratio between the concentrations of the solute on the two sides of the interface. Thus one obtains the following standard model:

Two-phase flow model $(1) - (4)$ combined with:

$$\frac{\partial c}{\partial t} + \mathbf{u} \cdot \nabla c = \operatorname{div}(D_i \nabla c) \quad \text{in } \Omega_i, \quad i = 1, 2, \tag{8}$$

$$[D_i \nabla c \cdot \mathbf{n}]_\Gamma = 0 \quad \text{on } \Gamma, \tag{9}$$

$$c_1 = C_H c_2 \quad \text{on } \Gamma. \tag{10}$$

The diffusion coefficient D_i is piecewise constant and in general $D_1 \neq D_2$. In the interface condition we use the notation c_i for $c_{|\Omega_i}$ restricted to the interface. The constant $C_H > 0$ is given (Henry's constant). The Henry interface condition can also be written as $[\hat{C}c]_\Gamma = 0$, with $\hat{C} = 1$ in Ω_1, $\hat{C} = C_H$ in Ω_2. The model has to be combined with suitable initial and boundary conditions. In the formulation in (8) there is a coupling between fluid dynamics and mass transport only *in one direction*, in the sense that the velocity is used in the mass transport equation, but the concentration c does *not* influence the fluid dynamics. In certain more complex systems it may be appropriate to consider a dependence of the surface tension coefficient on c, i. e., $\tau = \tau(c)$. In that case there is a coupling *in two directions* between fluid dynamics and mass transport. The functional form of $\tau = \tau(c)$ should be derived from interfacial rheology.

2.3 Surfactant transport

We consider a two-phase flow problem as described above in Section 2.1. We assume that there is a species (called tenside or surfactant) which adheres to the interface and is transported at the interface due to convection (movement of the interface) and due to diffusion (molecular diffusion on the interface). For simplicity we assume that there are no adsorption and desorption effects (i. e., no sources or sinks). The concentration of this surfactant is denoted by $S(x,t)$, $x \in \Gamma(t)$. From the conservation of mass principle and the constitutive law $q = -D_\Gamma \nabla_\Gamma S$ for the diffusive flux q, one obtains that

$$\int_\gamma \dot{S} + S \operatorname{div}_\Gamma \mathbf{u} + \operatorname{div}_\Gamma q \, ds = 0$$

must hold for an arbitrary connected subset $\gamma \subset \Gamma$, cf. Fig. 1. Here $\dot{S}$ denotes the material derivative of S. Hence we obtain the following model for transport of surfactants:

$$\text{Two-phase flow model } (1)-(4) \text{ combined with:}$$
$$\dot{S} + S \operatorname{div}_\Gamma \mathbf{u} = \operatorname{div}_\Gamma (D_\Gamma \nabla_\Gamma S) \quad \text{on } \Gamma. \tag{11}$$

If the diffusion coefficient D_Γ is constant on Γ we can reformulate the diffusion part as $\operatorname{div}_\Gamma(D_\Gamma \nabla_\Gamma S) = D_\Gamma \Delta_\Gamma S$. Using the definition of the material derivative the convection-diffusion equation in (11) can be written as

$$\frac{\partial S}{\partial t} + \mathbf{u} \cdot \nabla S + S \operatorname{div}_\Gamma \mathbf{u} = D_\Gamma \Delta_\Gamma S \quad \text{on } \Gamma.$$

In this formulation, for the partial derivatives $\frac{\partial}{\partial t}$ and $\mathbf{u} \cdot \nabla$ to be well-defined, one assumes that S is smoothly extended in a small neighborhood of Γ. For this surfactant transport equation no boundary conditions are needed if the interface Γ is a surface without boundary. In case of a stationary interface, i. e., $\mathbf{u} \cdot \mathbf{n} = 0$ on Γ, we have $\mathbf{P}\mathbf{u} = \mathbf{u}$ and thus $\mathbf{u} \cdot \nabla S + S \operatorname{div}_\Gamma \mathbf{u} = \mathbf{u} \cdot \nabla_\Gamma S + S \operatorname{div}_\Gamma \mathbf{u} = \operatorname{div}_\Gamma(\mathbf{u} S)$. Hence, we obtain the (simplified) diffusion equation $\frac{\partial S}{\partial t} + \operatorname{div}_\Gamma(\mathbf{u}S) - D_\Gamma \Delta_\Gamma S = 0$.

In the formulation in (11) there is a coupling between fluid dynamics and surfactant transport only *in one direction*, in the sense that the velocity is used in the surfactant transport equation, but the surfactant concentration S does *not* influence the fluid dynamics. In many systems with surfactants, there is a dependence of the surface tension coefficient on S, i. e., $\tau = \tau(S)$. In that case there is a coupling *in two directions* between fluid dynamics and surfactant transport Again, the functional form $\tau = \tau(S)$ has to be derived from interfacial rheology. In case of adsorption and desorption effects, we have additional source terms in (11). A (constitutive) model for these source terms has to be provided by research on interfacial rheology.

3 Interface representation

We consider the Navier-Stokes model for the two-phase fluid dynamics explained in Section 2.1. The dynamics of the interface is determined by the condition $V_\Gamma = \mathbf{u}\cdot\mathbf{n}_\Gamma$, which, however, describes the dynamics in a strongly implicit way, since the velocity field $\mathbf{u}$ depends on the location of the interface. In numerical simulations there are different strategies to deal with this problem. These strategies are closely related to different ways of representing the interface. Well-known methods are *interface tracking*, the *Volume of Fluid* (VOF) method, the *level set* (LS) method and the *phase field* method. For a treatment of these methods we refer to the literature, e.g. [21,16,26,12]. Here we only outline the key ideas underlying these different interface representation methods.

Interface tracking method. This method is conceptually very simple. The key idea is to describe the evolution of the interface using Lagrangian coordinates. Take a (virtual) particle $\mathbf{X}$ on the interface at $t = t_0$ with Eulerian coordinates $\xi \in \Gamma(t_0)$. For $t \geq t_0$, let $X_\xi(t)$ be the Eulerian coordinates of this particle. The particles on the interface are transported by the flow field, hence for $X_\xi(t)$ we have the ODE system

$$\begin{cases} \frac{d}{d\tau} X_\xi(\tau) = \mathbf{u}(X_\xi(\tau),\tau), \quad \tau \geq 0, \\ X_\xi(0) = \xi, \end{cases} \tag{12}$$

which determines the path of a material particle with initial position ξ. The interface $\Gamma(t)$ can be characterized as follows:

$$x \in \Gamma(t) \;\Leftrightarrow\; x = \xi + \int_{t_0}^{t} \mathbf{u}(X_\xi(\tau),\tau)\, d\tau, \quad \xi \in \Gamma(t_0), \quad t \geq t_0. \tag{13}$$

This interface representation forms the basis of the interface tracking methods. In these methods a collection of markers is put on a given interface $\Gamma(t_0)$ and then transported (numerically) by the flow field $\mathbf{u}$ to obtain the markers on the interface $\Gamma(t_0 + \Delta t)$. The collection of markers on $\Gamma(t_0)$ could be the set of vertices of a triangulation of $\Gamma(t_0)$. In such methods one usually has to redistribute the markers after a certain number of time steps. In general it is rather difficult to treat topology changes (e.g. collision of droplets) in a systematic and accurate way.

VOF method. This method can be classified as a *volume* tracking method, in the sense that one tries to determine the evolution of the characteristic function corresponding to the subdomain $\Omega_1(t)$. This function is denoted by $\chi_1 = \chi_1(t)$, i. e., $\chi_1(x) = 1$ if $x \in \Omega_1(t)$ and $\chi_1(x) = 0$ otherwise. Note that χ_1 is discontinuous across the interface $\Gamma(t)$. For an incompressible fluid mass conservation is equivalent to volume conservation. Let $W \subset \Omega$ be an arbitrary fixed (small) fluid volume. Volume conservation (in W) means that the change of volume of fluid 1 (i. e., the one in Ω_1) contained in W equals the volume flux (induced by the velocity field $\mathbf{u}$) across the boundary ∂W. This leads to the relation

$$\frac{\partial}{\partial t} \int_W \chi_1 \, dx + \int_{\partial W} \chi_1 \mathbf{u}\cdot\mathbf{n}\, ds = 0. \tag{14}$$

Here $\mathbf{n}$ denotes the outward unit normal on ∂W. In VOF methods one constructs approximations of the characteristic function χ_1 based on discretization of the conservation law (14). The VOF technique is very popular (in particular in the engineering community) and many variants have been developed, cf. [26]. VOF is often combined with finite volume discretization methods.

Level set method. Similar to the VOF method the level set technique is a volume tracking method, but instead of the characteristic function χ_1 it uses another indicator function. In the level set approach a *smooth* initial function $\phi_0(x),\ x \in \Omega$ is chosen such that

$$\phi_0(x) < 0 \ \Leftrightarrow\ x \in \Omega_1(0), \quad \phi_0(x) > 0 \ \Leftrightarrow\ x \in \Omega_2(0), \quad \phi_0(x) = 0 \ \Leftrightarrow\ x \in \Gamma(0).$$

A popular choice is to take ϕ_0 (approximately) equal to a signed distance function to the initial interface, cf. Fig. 2.

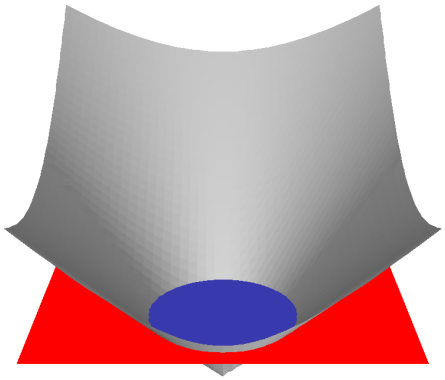

Fig. 2. Initial level set function ϕ_0 equals a signed distance function, 2D example.

A (virtual) particle $\mathbf{X}$ with Eulerian coordinates $\xi \in \Omega$ has a corresponding indicator value $\phi_0(\xi)$. Let $X_\xi(t),\ \xi \in \Omega$ be the characteristics (or particle paths) as defined in (12). For $t > 0$ the level set function values $\phi(x,t)$ are defined by keeping the values constant along characteristics, i. e.,

$$\phi(X_\xi(t), t) := \phi_0(\xi), \quad \xi \in \Omega,\ t \geq 0.$$

Differentiating this with respect to t results in the transport equation

$$\frac{\partial \phi}{\partial t} + \mathbf{u} \cdot \nabla \phi = 0 \quad \text{in } \Omega,\ t \geq 0. \tag{15}$$

The interface $\Gamma(t)$ *can be characterized by values of the level set function* at time t:

$$\Gamma(t) = \{\, x \in \Omega :\ \phi(x,t) = 0 \,\}. \tag{16}$$

Such a characterization of Γ by a level set of the indicator function is not possible in the VOF method, which uses the characteristic function as indicator. For the linear hyperbolic partial differential equation in (15), besides the initial condition one needs suitable boundary conditions, for example, a Dirichlet boundary condition $\phi(x,t) = \phi_D(x)$ on the inflow boundary $\partial\Omega_{in} := \{\, x \in \partial\Omega :\ \mathbf{u} \cdot \mathbf{n}_\Omega < 0 \,\}$. In the level set method one solves the level set equation (15) numerically (by, e.g., a finite volume or a finite element method). The interface is captured *implicitly* as the zero level of the numerical solution. During the evolution of the level set function ϕ (or of its discrete approximation), which is driven by the velocity field $\mathbf{u}$, the property of ϕ being close to a signed distance function is lost. This has undesirable effects, which can be avoided by using a so-called re-initialization technique. The issue of how to apply a re-initialization that restores the signed distance property while not changing the zero level too much plays an important role in the level set technique [21,16].

Phase field method. In the interface representations treated above the interface is either tracked explicitly or "captured" implicitly as the discontinuity of a characteristic function or the zero level of an approximate signed distance function. In all three cases one typically has a *sharp interface*. There are, however, interface modeling approaches in which one *always has a non sharp or diffusive interface*. These so-called phase field models are based on the observation that even for two (macroscopically) immiscible fluids there is a very thin interfacial region in which partial mixing of the two fluids occurs. In this sense, the physical interface is not sharp but diffusive. The interfacial mixing region has nonzero thickness but is extremely thin (typically $100\,nm$ or less). Hence modeling it as a sharp interface (as is done in the methods discussed above) seems reasonable. There are, however, mechanisms, for example in droplet collision, that are relevant and act on length scales comparable to that of interface thickness. For an accurate modeling of these mechanisms a diffusive interface representation may be more appropriate. Quantities that in the sharp interface formulation are localized at the interface, such as surface tension or surfactant transport, are distributed in a narrow interfacial region in a phase field model. The idea of diffusive interface modeling is an old one and was already used in [17,27]. An overview on diffusive interface methods is given in [2]. Apart from the difference sharp/diffusive another important difference between the methods presented above and the phase field method is that in the latter the indicator function has a physical meaning. One very important phase field model is due to Cahn-Hilliard. In this model one introduces an order parameter (indicator function) $c = c(x,t)$ that denotes a concentration and is scaled such that $c \in [-1,1]$ and $c(x,t) \approx -1$ corresponds to $x \in \Omega_1(t)$ and $c(x,t) \approx 1$ corresponds to $x \in \Omega_2(t)$. For this concentration one can derive a convection-diffusion equation of the form

$$\frac{\partial c}{\partial t} + \mathbf{u} \cdot \nabla c = m \Delta \mu^{\mathrm{chem}}, \quad \mu^{\mathrm{chem}} := \varepsilon^{-1} \psi_0'(c) - \varepsilon \Delta c, \tag{17}$$

with $m > 0$ the so-called mobility parameter, $\varepsilon > 0$ is a very small parameter that is related to the width of the transition layer (diffusive interface) between the two fluids and ψ_0 is a double well potential, e.g. $\psi_0(c) = (1-c^2)^2$. If we compare this with the level set approach we see that the level set function ϕ is replaced by the concentration c and the level set equation (15), which is a pure transport equation, is replaced by the convection-diffusion equation in (17). Recent work on numerical simulations of two-phase flows based on phase field models is presented in [23,24].

4 One-fluid model

As a basis for numerical simulations of two-phase flows one typically does *not* use a model with two Navier-Stokes equations in the two subdomains, as in (1), with coupling conditions as in (2), (3) and a dynamic condition as in (4). Instead one very often uses a *one-fluid* model, which we explain in this section. For the interface representation one uses one of the methods described in Section 3. As an example, we take the level set method. The level set equation describes the evolution of the interface, hence the condition (4) is not needed anymore. The jumps in the coefficients ρ and μ can be described using the level set function ϕ in combination with the Heaviside function $H : \mathbb{R} \to \mathbb{R}$:

$$H(\zeta) = 0 \quad \text{for } \zeta < 0, \qquad H(\zeta) = 1 \quad \text{for } \zeta > 0.$$

For ease one can set $H(0) = \frac{1}{2}$. We define

$$\begin{aligned} \rho(\phi) &:= \rho_1 + (\rho_2 - \rho_1) H(\phi), \\ \mu(\phi) &:= \mu_1 + (\mu_2 - \mu_1) H(\phi). \end{aligned} \tag{18}$$

The continuity condition in (3) is easy to satisfy by restricting to numerical approximations that are continuous. The important stress balance condition (2) can be reformulated as a *localized force term in the momentum equation*. Based on these observations the model (1)-(4) can be reformulated as follows:

$$\begin{cases} \rho(\phi)\big(\dfrac{\partial \mathbf{u}}{\partial t} + (\mathbf{u}\cdot\nabla)\mathbf{u}\big) = \operatorname{div}\boldsymbol{\sigma}(\phi) + \rho(\phi)\mathbf{g} + \delta_\Gamma \operatorname{div}_\Gamma \boldsymbol{\sigma}_\Gamma & \text{in } \Omega, \qquad (19) \\ \operatorname{div}\mathbf{u} = 0 \end{cases}$$

$$\frac{\partial \phi}{\partial t} + \mathbf{u}\cdot\nabla\phi = 0 \qquad \text{in } \Omega, \qquad (20)$$

with $\boldsymbol{\sigma}(\phi) := -p\mathbf{I} + \mu(\phi)\big(\nabla\mathbf{u} + (\nabla\mathbf{u})^T\big)$ and δ_Γ a suitable Dirac delta function that localizes the force $\operatorname{div}_\Gamma \boldsymbol{\sigma}_\Gamma$ on the interface. Note that in (19) we now have *one* Navier-Stokes equation in the whole domain Ω. Hence, this model is called the one-fluid model. Compared to the two Navier-Stokes equations in (1) the Navier-Stokes equation in (19) is more complicated, due to the discontinuities in viscosity μ and density ρ and the localized interface force term $\delta_\Gamma \operatorname{div}_\Gamma \boldsymbol{\sigma}_\Gamma$. To obtain a well-posed model one has to add suitable boundary and initial conditions for ϕ and $\mathbf{u}$. Note that the initial condition for ϕ determines the initial interface $\Gamma(0)$, due to (16).

Since the one-fluid model (where the level set method might be replaced by another interface representation method) is the basis of most numerical simulations in the literature, in the remainder we restrict to the model (19)-(20).

For a mathematical analysis of the model (19)-(20) and for certain numerical methods (cf. Section 6) one considers a suitable *weak formulation* of this model. For a treatment of this topic we refer to the literature, e.g. [12]. Here we only briefly address the weak formulation of the localized force term $\delta_\Gamma \operatorname{div}_\Gamma \boldsymbol{\sigma}_\Gamma$ since it often acts as an important driving force and an accurate numerical approximation is essential for numerical simulations. In a weak formulation of the momentum equation in (19) one multiplies the equation by suitable test functions $\mathbf{v} = \mathbf{v}(x) \in \mathbb{R}^3$ and integrates the equation over Ω. Due to the Dirac delta function δ_Γ, for the localized interface force the integration over Ω reduces to an integration over Γ. Thus one obtains the following *interface force functional* that models the interface force in a weak sense:

$$f_\Gamma(\mathbf{v}) = \int_\Gamma (\operatorname{div}_\Gamma \boldsymbol{\sigma}_\Gamma)\cdot\mathbf{v}\, ds \quad \text{with } \mathbf{v} \in \mathbf{V}, \qquad (21)$$

where $\mathbf{V}$ is a suitable class of test functions. A numerical approximation of this functional is discussed in Section 6.2.

5 Numerical challenges

The one-fluid model for modeling the fluid dynamics in a two-phase flow problem combined with the models for mass and surfactant transport discussed in the sections 2.2 and 2.3 poses enormous challenges to numerical simulation tools. Such flow models can not be solved reliably and accurately by the commercial codes that are available nowadays. Compared to *one*-phase flow solvers special tailor-made numerical methods have to be developed. Only recently the first monographs appeared in which numerical methods for two-phase incompressible flows are treated [12,26]. Below we address a few causes of the very high numerical complexity of this problem class.

Evolving unknown interface. The interface evolution is determined by the "simple" dynamic condition $V_\Gamma = \mathbf{u}\cdot\mathbf{n}$. The interface is a geometric object and it

turns out that an accurate numerical approximation of this object and its evolution is a very difficult task. In case of geometric singularities (e.g. droplet break up or collision) it becomes even more complicated. Although different techniques have been developed, cf. Section 3, an accurate interface approximation is still a challenging task.

Strong nonlinearities. The flow model contains several strongly nonlinear couplings. In the model (19)-(20) the transport of the level set function depends on the flow field $\mathbf{u}$. The latter is determined from the Navier-Stokes equation (19), but in this equation there is a strong dependence on (the zero level of) the level set function ϕ. This coupling between fluid dynamics, (19), and interface evolution, (20), turns out to be strongly nonlinear. A naive decoupling by simply iterating between the two equations is in general not a good procedure. If mass transport is considered and if there is a dependence of τ on the dilute concentration, i. e., $\tau = \tau(c)$, cf. Section 2.2, this coupling in two directions between fluid dynamics and mass transport is also in general strongly nonlinear. The same holds for a coupling in two directions between fluid dynamics and surfactant transport, i. e., $\tau = \tau(S)$. These strong nonlinearities cause difficulties for the construction of accurate numerical schemes for time discretization.

Moving discontinuities. In most applications the unknown interface is changing as a function of time. Many quantities are *discontinuous across the interface*. For example, the density and viscosity values have jumps across the interface. Due to surface tension forces the pressure is discontinuous across the interface. The force balance (2) and a jump in the viscosity across the interface typically induce a discontinuity across the interface of the normal derivative of the velocity. If mass transport is considered, then due to the Henry condition (10) the concentration c is discontinuous across the interface. If the VOF technique is used, the characteristic function χ_1, which is discontinuous across the interface, has to be determined. The numerical treatment of moving discontinuities (cf. also shocks in compressible flow problems) often causes severe difficulties.

PDEs on moving manifolds. The problem class that we consider gives rise to partial differential equations (PDEs) on the moving interface. An example is the surfactant transport equation (11). Another example comes from systems in which the interface has viscoelastic behavior. In such problems the constitutive model for the interface stress tensor $\boldsymbol{\sigma}_\Gamma$ often contains a partial differential equation on the interface, e.g. a Kelvin-Voigt type model [19]. The numerical solution of partial differential equations on moving manifolds is a difficult topic, which has been addressed in the literature only recently.

Efficient iterative solvers. After discretization in space and *implicit* discretization in time one obtains a very large nonlinear system of equations (for the discrete quantities) in each time step. In simulations by far most of the total computing time is needed for solving these large nonlinear systems. The efficiency of these iterative solvers can be strongly improved by using special techniques that are adapted to the problem class, in the sense that the solver makes use of certain structural properties of the problem. Until now there has been only very little research on this topic.

6 Finite element discretization techniques

In this section we treat a few numerical methods that address some of the challenges discussed in Section 5. We restrict to finite element techniques that have been studied in our group in recent years. We only present the main ideas of the methods, for more detailed treatments we refer to the literature. The methods discussed in this

section are implemented in the two-phase flow solver DROPS [6], which is used in the numerical experiments in Section 7.

6.1 Multilevel grid hierarchy

Clearly, since in a two-phase flow problem the interesting phenomena happen at (or close to) the interface, for the discretization of such a problem it is beneficial to use grids which have a (very) high resolution close to the interface compared to the resolution further away from the interface. A high resolution in the whole domain ("uniform grid") leads to a waste of computer memory and computational time. A high resolution close to the interface can be obtained by using locally refined grids. In most applications the interface is moving in time and thus the grids have to be adapted if time evolves. One needs numerical methods that are able to realize a *local refinement and local coarsening* (i. e., undo the refinement). In particular the local coarsening of a given grid is not an easy task. In our solver we use tetrahedral grids that are constructed in such a way that they are consistent (no hanging nodes) and stable (no small angles). To be able to realize local refinement and local coarsening in an efficient way the grids are constructed based on a *hierarchy of triangulations*. In such a hierarchy, which is called a multilevel grid hierarchy, one starts with a relatively coarse triangulation that is then (locally) refined several times. By storing the whole hierarchy (and not only the finest grid) it is easy to undo a refinement, i. e., to realize a coarsening. A detailed explanation of the methods and further properties are given in [12]. Examples of locally refined tetrahedral grids are shown in Fig. 7.

6.2 Laplace-Beltrami based discretization of interface forces

In many cases the forces at the interface, modeled by the interface stress tensor $\operatorname{div}_\Gamma \boldsymbol{\sigma}_\Gamma$, strongly influence the fluid dynamics. Therefore an accurate numerical treatment of these forces is of major importance. In the weak formulation the forces are modeled by the interface force functional $f_\Gamma(\mathbf{v}) = \int_\Gamma (\operatorname{div}_\Gamma \boldsymbol{\sigma}_\Gamma) \cdot \mathbf{v}\, ds$, cf. (21). In this section we explain a numerical method that yields an accurate discretization of this functional. The basis of this method is the following partial integration rule (that results from elementary differential geometry):

$$f_\Gamma(\mathbf{v}) = \int_\Gamma \operatorname{div}_\Gamma(\boldsymbol{\sigma}_\Gamma) \cdot \mathbf{v}\, ds = -\int_\Gamma \operatorname{tr}(\boldsymbol{\sigma}_\Gamma \nabla_\Gamma \mathbf{v})\, ds = -\sum_{i=1}^{3} \int_\Gamma (e_i \cdot \boldsymbol{\sigma}_\Gamma) \nabla_\Gamma v_i\, ds, \quad (22)$$

where $\operatorname{tr}(\cdot)$ denotes the trace of a matrix, $\mathbf{v} = (v_1, v_2, v_3)$ and e_i is the ith standard basis vector in $\mathbb{R}^3$. To explain the discretization of this functional we restrict ourselves to the case of a clean interface, i. e., $\boldsymbol{\sigma}_\Gamma = \tau \mathbf{P}$, with a constant surface tension coefficient τ. For this case the relations (22) result in

$$f_\Gamma(\mathbf{v}) = -\tau \int_\Gamma \kappa \mathbf{n} \cdot \mathbf{v}\, ds = -\tau \sum_{i=1}^{3} \int_\Gamma (\mathbf{P} e_i) \cdot \nabla_\Gamma v_i\, ds, \quad (23)$$

with κ the curvature of the interface. This partial integration rule is closely related to the following fundamental *Laplace-Beltrami characterization of the mean curvature*:

$$-\Delta_\Gamma \mathrm{id}_\Gamma(x) = \kappa(x)\mathbf{n}(x), \quad x \in \Gamma.$$

From the formula (23) one can see the advantage of the representation on the right-hand side compared to that on the left-hand side. In the latter one needs the curvature

of Γ (which is not easy to approximate accurately), whereas in the former we only need the projection $\mathbf{P} = \mathbf{I} - \mathbf{n}\mathbf{n}^T$. Thus as basis for the numerical method we use the representation on the right-hand side in (23). For the discretization of this integral we need a discrete approximation Γ_h of Γ. This can be constructed as follows. Let $\mathcal{T}_h$ be a tetrahedral triangulation of the domain Ω. For discretization of the level set equation we use piecewise *quadratic* finite elements, i. e., functions that are continuous on Ω and quadratic polynomials on each of the tetrahedra in the triangulation $\mathcal{T}_h$. We do not explain this discretization method here, but instead refer to [12]. The resulting discrete approximation of the level set function ϕ (at a given time t) is denoted by ϕ_h. The corresponding zero level $\left\{ x \in \mathbb{R}^3 : \phi_h(x) = 0 \right\}$ is difficult to compute and therefore the following *linear* approximation is introduced. We use a regular refinement of $\mathcal{T}_h$, denoted by $\mathcal{T}_h'$, which is obtained by regularly subdividing each tetrahedron of $\mathcal{T}_h$ into 8 child tetrahedra. Let $I(\phi_h)$ be the continuous piecewise *linear* function on $\mathcal{T}_h'$ which interpolates ϕ_h at all vertices of all tetrahedra in $\mathcal{T}_h'$. The approximation of the interface Γ is defined by

$$\Gamma_h := \{ x \in \Omega : I(\phi_h)(x) = 0 \} \tag{24}$$

and consists of piecewise planar segments, which are either triangles or quadrilaterals. This interface approximation is easy to compute. Let $\mathbf{n}_h$ be the unit normal on Γ_h (which is constant on each of the planar segments and not defined on the edges between the segments). The discrete projection corresponding to Γ_h is given by $\mathbf{P}_h = \mathbf{I} - \mathbf{n}_h\mathbf{n}_h^T$. An easy to compute discrete approximation of the interface force functional in (23) is given by

$$f_{\Gamma_h}(\mathbf{v}) := -\tau \sum_{i=1}^{3} \int_{\Gamma_h} (\mathbf{P}_h e_i) \cdot \nabla_{\Gamma_h} v_i \, ds. \tag{25}$$

An error analysis shows that the accuracy of this approximation is rather low [11]. A significant improvement is obtained by using the following simple modification, in which more information from the piecewise *quadratic* finite element approximation ϕ_h is used. We define an improved projection

$$\tilde{\mathbf{n}}_h(x) := \frac{\nabla \phi_h(x)}{\|\nabla \phi_h(x)\|}, \qquad \tilde{\mathbf{P}}_h(x) := \mathbf{I} - \tilde{\mathbf{n}}_h(x)\tilde{\mathbf{n}}_h(x)^T, \quad x \in \Gamma_h.$$

Note that this projection is easy to compute and does not need the zero level of ϕ_h. This results in the following discrete approximation of the interface force functional

$$\tilde{f}_{\Gamma_h}(\mathbf{v}) := -\tau \sum_{i=1}^{3} \int_{\Gamma_h} (\tilde{\mathbf{P}}_h e_i) \cdot \nabla_{\Gamma_h} v_i \, ds,$$

which turns out to be much more accurate than the one in (25). This discretization procedure can also be applied to a general interface force functional as in (22), i. e., with an interface stress tensor that differs from $\boldsymbol{\sigma}_\Gamma = \tau \mathbf{P}$.

6.3 XFEM technique

In cases with large surface tension forces the pressure has a large jump across the interface. In standard polynomial finite element spaces the functions may be discontinuous across element sides or faces, but they are continuous inside the elements. Due to the non-alignment the interface intersects many elements and thus such finite element functions are not appropriate for the approximation of the pressure, which

is discontinuous across the interface. In many simulations these effects cause large oscillations of the velocity close to the interface, so-called *spurious velocities*, cf. the results of the numerical experiment in Section 7.2.

The *extended* finite element method (XFEM) as presented in [14,4] allows a much better (even optimal) approximation of the discontinuous pressure. We explain the main idea of this XFEM technique for the discretization of the pressure variable. Let $\mathcal{T}_h$ be a triangulation of the domain Ω consisting of tetrahedra and let

$$Q_h = \{\, q \in C(\Omega) : q|_T \in \mathcal{P}_1 \quad \text{for all } T \in \mathcal{T}_h \,\}$$

be the standard finite element space of continuous piecewise linear functions. We define the index set $\mathcal{J} = \{1, \ldots, n\}$, where $n = \dim Q_h$ is the number of degrees of freedom. Let $\mathcal{B} := \{q_j\}_{j=1}^n$ be the nodal basis of Q_h, i. e., $q_j(\mathbf{x}_i) = \delta_{ij}$ for $i, j \in \mathcal{J}$ where $\mathbf{x}_i \in \mathbb{R}^3$ denotes the spatial coordinate of the i-th degree of freedom.

The idea of the XFEM is to enrich the original finite element space Q_h by additional basis functions q_j^X for $j \in \mathcal{J}'$ where $\mathcal{J}' \subset \mathcal{J}$ is a given index set. An additional basis function q_j^X is constructed by multiplying the original nodal basis function q_j by a so-called enrichment function Φ_j:

$$q_j^X(x) := q_j(x)\, \Phi_j(x). \tag{26}$$

This enrichment yields the *extended finite element space*

$$Q_h^X := \operatorname{span}\big(\{q_j\}_{j\in\mathcal{J}} \cup \{q_j^X\}_{j\in\mathcal{J}'}\big).$$

This idea was introduced in [14] and further developed in [4] for different kinds of discontinuities (kinks, jumps), which may also intersect or branch. The choice of the enrichment function depends on the type of discontinuity. For representing jumps the Heaviside function is proposed to construct appropriate enrichment functions. Basis functions with kinks can be obtained by using the distance function as enrichment function.

In our case the finite element space Q_h is enriched by discontinuous basis functions q_j^X for $j \in \mathcal{J}' := \{\, j \in \mathcal{J} : \operatorname{meas}_2(\Gamma \cap \operatorname{supp} q_j) > 0 \,\}$, as discontinuities in the pressure only occur at the interface. Let $d : \Omega \to \mathbb{R}$ be the signed distance function (or an approximation to it) with d negative in Ω_1 and positive in Ω_2. In our applications the discretization of the level set function φ is used for d. Then by means of the Heaviside function H we define

$$H_\Gamma(x) := H(d(x)) = \begin{cases} 0 & x \in \Omega_1 \cup \Gamma, \\ 1 & x \in \Omega_2. \end{cases}$$

As we are interested in functions with a jump across the interface we define the enrichment function

$$\Phi_j^H(x) := H_\Gamma(x) - H_\Gamma(\mathbf{x}_j) \tag{27}$$

and a corresponding function $q_j^X := q_j \cdot \Phi_j^H$, $j \in \mathcal{J}'$. The second term in the definition of Φ_j^H is constant and may be omitted (as it does not introduce new functions in the function space), but ensures the nice property $q_j^X(\mathbf{x}_i) = 0$, i. e., q_j^X vanishes in all degrees of freedom.

We use the notation $q_j^\Gamma := q_j\, \Phi_j^H$ and define

$$Q_h^\Gamma := \operatorname{span}(\{\, q_j : j \in \mathcal{J} \,\} \cup \{\, q_j^\Gamma : j \in \mathcal{J}_\Gamma \,\}) = Q_h \oplus \operatorname{span}\{\, q_j^\Gamma : j \in \mathcal{J}_\Gamma \,\}. \tag{28}$$

The superscript Γ is used to emphasize that the extended finite element space Q_h^Γ depends on the location of the interface Γ. In particular the dimension of Q_h^Γ may change if the interface is moved. The shape of the extended basis functions for the 1D case is sketched in Fig. 3.

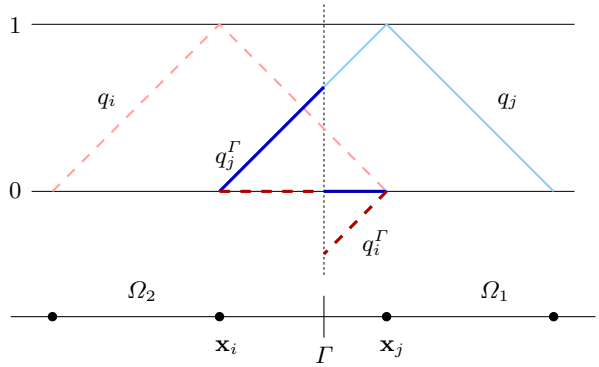

Fig. 3. Extended finite element basis functions q_i, q_i^Γ (dashed) and q_j, q_j^Γ (solid) for 1D case.

In [15] optimal approximation error bounds, both in the L^2 and H^1 norm, for this XFE space are derived. For example, for $p \in L^2(\Omega)$ with $p_{|\Omega_i} \in H^2(\Omega_i)$, $i = 1, 2$, we have

$$\inf_{q_h \in Q_h^\Gamma} \|q_h - p\|_{L^2} \leq ch^2 \|p\|_{2,\Omega_1 \cup \Omega_2}. \tag{29}$$

In [15] a variant is introduced in which discontinuous basis functions that were originally added in the *extended* finite element space are left out if they have a "very small" support. This cut-off technique leads to a modified XFE space with the same (optimal) approximation quality as the original XFE space but with (much) better stability properties.

The XFE space defined in (28) or other XFE spaces (with other enrichment functions) are used not only in simulations of two-phase flows (with a discontinuous pressure) but also in other application areas, e.g. crack propagation in mechanics [9,10].

6.4 Space-time finite elements

As discussed in Section 5, an important challenge in two-phase flow simulations comes from the fact that we have to deal with *moving* discontinuities. In Section 6.3 we outlined the XFEM technique for approximation of the discontinuous pressure at a given (fixed) time t. The time dependence of the discontinuity can be treated by a so-called *space-time* finite element technique. Since the pressure is part of the Navier-Stokes equations one would have to combine the XFEM technique with a space-time approach for the Navier-Stokes equations. As far as we know, this has not been studied in the literature, yet. A moving discontinuity also occurs in the mass transport equation (8), which is only a *scalar* convection-diffusion equation (and thus is much simpler than the Navier-Stokes equation). Recently an XFE-space-time method for this mass transport equation has been introduced and analyzed in [13]. In this section we explain the idea of this method. For this, we first explain the basic concept of the space-time finite element method (no XFEM) for a problem with a smooth solution,

namely the model parabolic problem

$$\begin{aligned} \frac{\partial u}{\partial t} - \Delta u &= f \quad \text{in } \Omega,\ t \in [0,T], \\ u(\cdot,0) &= u_0 \quad \text{in } \Omega, \\ u(\cdot,t) &= 0 \quad \text{on } \partial\Omega. \end{aligned} \tag{30}$$

For simplicity we assume f to be independent of t. We use a partitioning of the time domain $0 = t_0 < t_1 < \ldots < t_N = T$, with a fixed time step size $\Delta t = T/N$, i. e., $t_j = j\Delta t$. This assumption of a fixed time step is made to simplify the presentation, but is *not* essential for the method. Corresponding to each time interval $I_n := (t_{n-1}, t_n)$ we have a consistent triangulation $\mathcal{T}_n$ of the domain Ω. This triangulation may vary with n. Let V_n be a finite element space of continuous piecewise polynomial functions corresponding to the triangulation $\mathcal{T}_n$, with boundary values equal to zero. For $1 \le n \le N$ and a nonnegative integer k we define, on each time slab $Q^n := \Omega \times I_n$, a space-time finite element space as follows:

$$V_{kn} := \left\{ v : Q^n \to \mathbb{R} :\ v(x,t) = \sum_{j=0}^{k} t^j \phi_j(x),\ \phi_j \in V_n \right\}, \tag{31}$$

for $1 \le n \le N$. The corresponding space-time discretization of (30) reads: Determine u_h such that for all $n = 1, 2, \ldots, N$, $(u_h)_{|Q^n} \in V_{kn}$ and

$$\begin{aligned} &\int_{t_{n-1}}^{t_n} \big(\frac{\partial u_h}{\partial t}, v_h\big)_{L^2} + (\nabla u_h, \nabla v_h)_{L^2}\, dt + ([u_h]^{n-1}, v_h^{n-1,+})_{L^2} \\ &= \int_{t_{n-1}}^{t_n} (f, v_h)_{L^2}\, dt \quad \text{for all } v_h \in V_{kn}, \end{aligned} \tag{32}$$

where $(\cdot,\cdot)_{L^2} = (\cdot,\cdot)_{L^2(\Omega)}$,

$$[w_h]^n = w_h^{n,+} - w_h^{n,-}, \quad w_h^{n,+(-)} = \lim_{s \to 0^{+(-)}} w_h(\cdot, t_n + s),$$

and $u_h^{0,-} \in V_1$ an approximation of the initial data u_0. Such space-time finite element methods for parabolic problems are well-known in the literature. For an analysis and further explanation of this discretization method we refer to the literature, e.g. [25].

As examples, we consider two important special cases, namely $k = 0$, $k = 1$. If $k = 0$ then $v_h \in V_{kn}$ does not depend on t. Define $u_h^n(x) := u_h(x,t)$, $t \in I_n$. The method (32) for determining $u_h^n \in V_n$ reduces to the implicit Euler scheme:

$$\frac{1}{\Delta t}(u_h^n - u_h^{n-1}, v_h)_{L^2} + (\nabla u_h^n, \nabla v_h)_{L^2} = (f, v_h)_{L^2} \quad \text{for all } v_h \in V_n.$$

We now consider $k = 1$. Then on Q^n the function u_h^n can be represented as $u_h^n(x,t) = \hat{u}_h^n(x) + \frac{1}{\Delta t}(t - t_{n-1})\tilde{u}_h^n(x)$, with $\hat{u}_h^n$, $\tilde{u}_h^n \in V_n$. These unknown functions are uniquely determined by the coupled system

$$\begin{aligned} (\hat{u}_h^n + \tilde{u}_h^n, v_h)_{L^2} + \Delta t\big(\nabla \hat{u}_h^n + \frac{1}{2}\nabla \tilde{u}_h^n, \nabla v_h\big)_{L^2} &= (u_h^{n-1,-}, v_h)_{L^2} + \Delta t (f, v_h)_{L^2}, \\ \frac{1}{2}(\tilde{u}_h^n, v_h)_{L^2} + \Delta t\big(\frac{1}{2}\nabla \hat{u}_h^n + \frac{1}{3}\nabla \tilde{u}_h^n, \nabla v_h\big)_{L^2} &= \frac{1}{2}\Delta t (f, v_h)_{L^2}, \end{aligned}$$

for all $v_h \in V_n$, cf. [25].

We now explain how a space-time approach can be combined with the XFE technique for the mass transport equation (8), which has a solution with a moving discontinuity. The key idea is to use a space-time discretization as in (32) but with the space V_{kn} replaced by a suitable space-time *extended* finite element space. We explain this space more precisely for the case of finite elements that are piecewise *linear w.r.t. space and time*. Let V_n be the finite element space of continuous piecewise *linear* functions on $\mathcal{T}_n$ with zero boundary values on $\partial\Omega$. Corresponding spaces of piecewise linear space-time finite element functions on the time slab Q^n are given by

$$W_n := \{\, v : Q^n \to \mathbb{R} :\ v(x,t) = \phi_0(x) + t\phi_1(x), \quad \phi_0, \phi_1 \in V_n \,\}. \tag{33}$$

We introduce a space-time XFE space based on similar ideas as explained in Section 6.3. Let $\{q_j\}_{j\in\mathcal{J}}$ be the nodal basis in the finite element space V_n. The vertex corresponding to q_j is denoted by $\mathbf{x}_j$. To each q_j there correspond two space-time basis functions, namely $q_{j,0}(x,t) := \frac{1}{\Delta t}(t_n - t)q_j(x)$ and $q_{j,1}(x,t) := \frac{1}{\Delta t}(t - t_{n-1})q_j(x)$.The index set of basis functions in the space-time finite element space W_n "close to the interface" is given by

$$\mathcal{J}_{\Gamma_*^n} := \big\{\, (j,0),(j,1) :\ \mathrm{meas}_3\big(\Gamma_*^n \cap \mathrm{supp}(q_j)\big) > 0 \,\big\},$$

where Γ_*^n denotes the space-time interface in Q^n, i. e., $\Gamma_*^n := \cup_{t\in I_n}\Gamma(t)$. For a 1D example, the vertices corresponding to this index set are illustrated in Fig. 4.

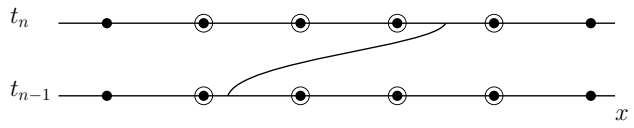

Fig. 4. Enrichment index set for 1D example. Dots represent degrees of freedom of original basis functions, circles indicate where additional functions are added with indices in enrichment index set $\mathcal{J}_{\Gamma_*^n}$.

Define $Q_2^n := \{\, (x,t) \in Q^n :\ x \in \Omega_2(t) \,\}$ and let $H_{\Gamma_*^n}$ be the characteristic function corresponding to Q_2, i. e., $H_{\Gamma^n}(x,t) = 1$ if $(x,t) \in Q_2^n$ and zero otherwise. For each space-time node index $(j,\ell) \in \mathcal{J}_{\Gamma_*^n}$ a so-called enrichment function corresponding to the node $(x_j, t_{n-\ell})$ is given by

$$\Phi_{j,\ell}(x,t) := H_{\Gamma_*^n}(x,t) - H_{\Gamma_*^n}(\mathbf{x}_j, t_{n-\ell}). \tag{34}$$

New basis functions are defined as follows:

$$q_{j,\ell}^{\Gamma_*^n} := q_{j,\ell}\Phi_{j,\ell}, \quad (j,\ell) \in \mathcal{J}_{\Gamma_*^n}. \tag{35}$$

The term $H_{\Gamma_*^n}(\mathbf{x}_j, t_{n-\ell})$ in the definition of $\Phi_{j,\ell}$ is constant and may be omitted (as it doesn't introduce new functions in the function space), but ensures that $q_{j,\ell}^{\Gamma_*^n}(\mathbf{x}_j, t_{n-\ell}) = 0$ holds in all space-time grid points $(\mathbf{x}_j, t_{n-\ell})$. The space-time XFE space on the time slab Q^n is given by

$$W_n^\Gamma = W_n \oplus \mathrm{span}\left\{\, q_{j,\ell}^{\Gamma_*^n} :\ (j,\ell) \in \mathcal{J}_{\Gamma_*^n} \,\right\}.$$

Hence, the XFE space W_n^Γ is obtained by adding to the standard space W_n new basis functions that are discontinuous across the space-time interface Γ_*^n, cf. (35). An XFEM-space-time discretization of the mass transport equation is obtained by taking a variational formulation of (8), similar to (32), but with trial and test functions from the space W_n^Γ. This is explained and analyzed in [13]. In that paper one can also find an approach for the numerical treatment of the Henry interface condition in (10).

6.5 Discretization of a PDE on the interface

In this section we briefly address the numerical solution of partial differential equations on (evolving) interfaces. Until recently this topic has hardly been studied, but in the past few years several conceptually different finite element techniques have been proposed. As an illustration we first consider two of these techniques for the case of a *stationary* interface. We then discuss methods for the case of a moving interface.

Stationary interface. For simplicity, instead of a surfactant equation we consider a pure surface diffusion equation, the so-called Laplace-Beltrami equation:

$$-\Delta_\Gamma u = f \quad \text{on } \Gamma. \tag{36}$$

To obtain a well-posed problem we assume that $\int_\Gamma f\,ds = 0$ holds. The first finite element method for this problem is introduced in [7]. We explain this method. The surface Γ is approximated by a *shape-regular* family $\{\mathcal{G}_h\}_{h>0}$ of triangulations. Each triangulation $\mathcal{G}_h$ is consistent (no hanging nodes) and it is assumed that all vertices in the triangulation lie on Γ. The space of scalar functions that are continuous on the approximated surface $\Gamma_h := \bigcup_{F\in\mathcal{G}_h} F$ and linear on each triangle in the triangulation $\mathcal{G}_h$ is denoted by V_h. The discretization of the Laplace-Beltrami equation is as follows: determine $u_h \in V_h$ with $\int_{\Gamma_h} u_h\,ds = 0$ and such that

$$\int_{\Gamma_h} \nabla_{\Gamma_h} u_h \cdot \nabla_{\Gamma_h} v_h \; ds = \int_{\Gamma_h} f_h v_h \; ds \qquad \text{for all } v_h \in V_h. \tag{37}$$

Here $\nabla_{\Gamma_h} = \mathbf{P}_h\nabla$ is the tangential derivative corresponding to Γ_h and f_h a suitable extension of the data f. An analysis of this method is given in [7].

A conceptually very different method is the following one, from [15]. Let $\{\mathcal{T}_h\}_{h>0}$ be a shape-regular family of tetrahedral triangulations of a *fixed* domain $\Omega \subset \mathbb{R}^3$ that contains Γ. Take $\mathcal{T}_h \in \{\mathcal{T}_h\}_{h>0}$. We need an approximation Γ_h of Γ and assume that this approximate interface has the following properties. We assume that Γ_h is a $C^{0,1}$ surface without boundary and that Γ_h can be partitioned in planar segments, triangles or quadrilaterals, consistent with the outer triangulation $\mathcal{T}_h$. This can be formally defined as follows. For any tetrahedron $S_F \in \mathcal{T}_h$ such that $\mathrm{meas}_2(S_F \cap \Gamma_h) > 0$ define $F = S_F \cap \Gamma_h$. We assume that each F is *planar*, i. e., either a triangle or a quadrilateral. Thus, Γ_h can be decomposed as

$$\Gamma_h = \bigcup_{F\in\mathcal{F}_h} F, \tag{38}$$

where $\mathcal{F}_h$ is the set of all triangles or quadrilaterals F such that $F = S_F \cap \Gamma_h$ for some tetrahedron $S_F \in \mathcal{T}_h$.

The construction of Γ_h as described in Section 6.2, cf. (24), satisfies the assumptions made above. An illustration is shown in Fig. 5.

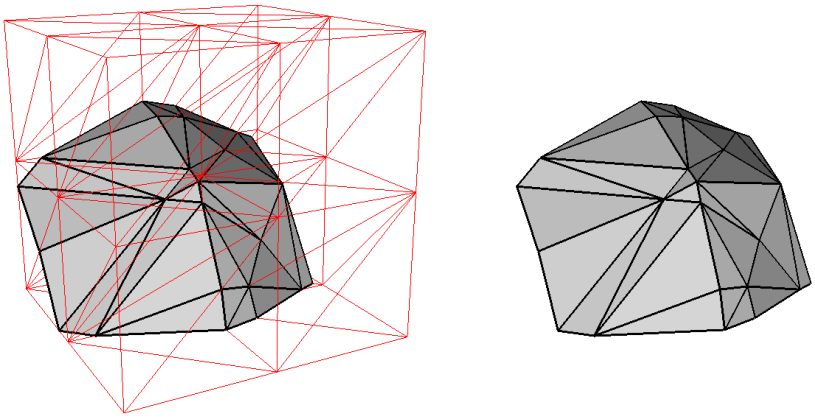

Fig. 5. Detail of the interface triangulation Γ_h. On the left, also the outer triangulation $\mathcal{T}_h'$ is shown.

Note that this construction in general results in an interface triangulation that is very shape *ir*regular. For discretization of the problem (36) we use a finite element space induced by the continuous linear finite elements on $\mathcal{T}_h$. This is done as follows. We define a subdomain $\omega_h \subset \Omega$ that contains Γ_h,

$$\omega_h := \bigcup_{F \in \mathcal{F}_h} S_F, \tag{39}$$

and introduce the finite element space

$$V_h := \left\{ v_h \in C(\omega_h) : v_{|S_F} \in \mathcal{P}_1 \quad \text{for all } F \in \mathcal{F}_h \right\}. \tag{40}$$

This space induces the following space on Γ_h:

$$V_h^{\Gamma_h} := \left\{ \psi_h \in H^1(\Gamma_h) : \exists\, v_h \in V_h : \psi_h = v_h|_{\Gamma_h} \right\}. \tag{41}$$

The spaces V_h and $V_h^{\Gamma_h}$ are called *outer* and *surface* finite element space, respectively. The surface space is used for the discretization of (36): determine $u_h \in V_h^{\Gamma_h}$ with $\int_{\Gamma_h} u_h \, ds = 0$ such that

$$\int_{\Gamma_h} \nabla_{\Gamma_h} u_h \cdot \nabla_{\Gamma_h} \psi_h \, ds = \int_{\Gamma_h} f_h \psi_h \, ds \qquad \text{for all } \psi_h \in V_h^{\Gamma_h}, \tag{42}$$

with f_h a suitable extension of f. This method is particularly suitable for problems in which the interface is given implicitly by a level set or VOF function and in which there is a coupling with a flow problem in a fixed outer domain, as is the case in two-phase flow problems. If in such problems one uses finite element techniques for the discretization of the flow equations in the outer domain, this setting immediately results in an easy to implement discretization method for the surface equation. If the surface varies in time, one has to recompute the surface mass and stiffness matrix using the same data structures each time. Quadrature routines that are needed for these computations are often available already, since they are needed in other surface related calculations, for example surface tension forces.

Non-stationary interface. The state of affairs concerning discretization methods for solving partial differential equations on moving interfaces is not very satisfactory. Existing methods all have certain (severe) drawbacks and further research is needed. In [8] the method (37) is generalized to problems with a non-stationary interface. A generalization of the method (42) to moving interfaces is proposed in [12].

6.6 Further discussion

In the sections 6.1–6.5 we discussed a few methods that have been used to develop the two-phase flow solver DROPS. We emphasize, however, that for the development of this (or another) two-phase flow solver also (many) other computational components are essential. We mention a few. The use of *appropriate time discretization methods* is of major importance. These methods should be stable and sufficiently accurate. Due to the large stiffness of the differential equations involved implicit methods are required. This leads to highly nonlinear discrete problems that have to be solved in each time step. For this one has to develop suitable *linearization techniques*. These linearization methods result in very large sparse linear systems of equations. These systems have to be solved by *fast iterative solvers*. These solvers can be based on Krylov subspace techniques and multigrid methods. Often suitable so-called *preconditioners* have to be developed. *Error estimators* are needed to control the adaptation of the spatial grid and the time step length. For the level set technique, besides the re-initialization, an appropriate *mass conservation* is an important issue. Even if one uses very efficient tools, due to the enormous complexity of many two-phase flow problems (coupled with mass or surfactant transport) a *parallelization* of the code is required. Here suitable *load balancing strategies* accounting for the moving interface are crucial.

7 Examples of numerical experiments

In this section we present results of a few numerical experiments with the two-phase flow solver DROPS [6]. We restrict ourselves to the fluid-dynamics, i. e., the Navier-Stokes model given in Section 4. For examples of simulations with mass or surfactant transport we refer to [12]. In the first example, in Section 7.1, we consider the fluid dynamics of a rising n-butanol droplet in water with a clean interface, i. e., only surface tension forces modeled by $\boldsymbol{\sigma}_\Gamma = \tau \mathbf{P}$. In the second example, in Section 7.2, we take a toluene-water system with a clean interface, which has a much larger surface tension than the n-butanol-water system. We illustrate that the use of the XFE technique for pressure discretization results in strongly reduced spurious velocities compared to the standard finite element method. Finally, in Section 7.3 we consider an artificial system with a spherical droplet transported in a Poisseuille flow, but with viscous interface forces modeled by the Boussinesq-Scriven constitutive law.

7.1 Rising butanol droplet with clean interface model

We present results, taken from [12], of a numerical experiment with a single n-butanol droplet inside a rectangular tank $\Omega = [0, 12 \cdot 10^{-3}] \times [0, 30 \cdot 10^{-3}] \times [0, 12 \cdot 10^{-3}]\, m^3$ filled with water, cf. Fig. 6. The material properties of this two-phase system are given in Table 1. An initially spherical droplet that is at rest ($\mathbf{u}_0 = 0\, m/s$) starts to rise in y-direction due to buoyancy effects, with $y = x_2$ and $x = (x_1, x_2, x_3)$. The numerical simulation is based on the one-fluid model described in Section 4, with a clean interface stress tensor $\boldsymbol{\sigma}_\Gamma = \tau \mathbf{P}$.

Table 1. Material properties of the system n-butanol / water.

quantity (unit)		n-butanol	water
ρ	(kg/m^3)	845.4	986.5
μ	$(kg/m\,s)$	$3.281 \cdot 10^{-3}$	$1.388 \cdot 10^{-3}$
τ	(N/m)	$1.63 \cdot 10^{-3}$	

Table 2. Material properties of the system toluene / water.

quantity (unit)		toluene	water
ρ	(kg/m^3)	867.5	998.8
μ	$(kg/m\,s)$	$5.96 \cdot 10^{-4}$	$1.029 \cdot 10^{-3}$
τ	(N/m)	$34.31 \cdot 10^{-3}$	

For the initial triangulation $\mathcal{T}_0$ the domain Ω is subdivided into $4\times10\times4$ sub-cubes each consisting of 6 tetrahedra. Then the grid is refined four times in the vicinity of the interface Γ. As time evolves the grid is adapted to the moving interface. Fig. 7 shows the droplet and a part of the adaptive mesh for two different time steps. The velocity space $\mathbf{V}_h$ consists of piecewise quadratics and the pressure is discretized using the XFEM space $Q_h^{\Gamma_h}$, cf. Section 6.3. The modified Laplace-Beltrami discretization (cf. Section 6.2) is applied for the surface tension force term. The level set function is discretized by piecewise quadratics and streamline-diffusion stabilization.

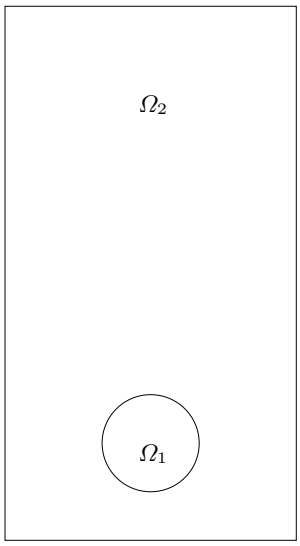

Fig. 6. 2D sketch of the rising droplet example.

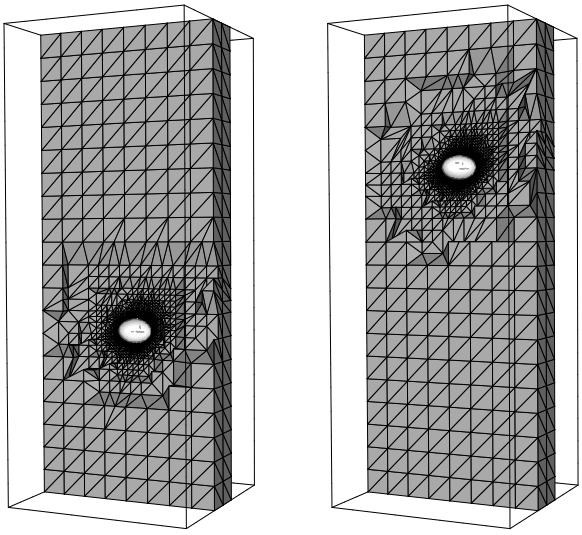

Fig. 7. Interface and part of the grid for a rising droplet with radius $r_d = 1\,mm$ at times $t = 0.2\,s$ (left) and $t = 0.4\,s$ (right).

For a butanol droplet with radius $1\,mm$, in Fig. 8 the y-coordinate of the droplet's barycenter $\overline{x}_d$ is shown as a function of time, where

$$\overline{x}_d(t) = \mathrm{vol}(\Omega_1(t))^{-1} \int_{\Omega_1(t)} x\,dx.$$

The average velocity $\overline{\mathbf{u}}_d(t)$ of the drop is given by

$$\overline{\mathbf{u}}_d(t) = \mathrm{vol}(\Omega_1(t))^{-1} \int_{\Omega_1(t)} \mathbf{u}(x,t)\,dx.$$

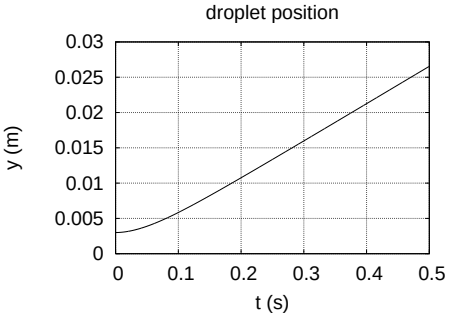

Fig. 8. y-coordinate of barycenter of a rising butanol droplet with radius $1\,mm$ as a function of time t.

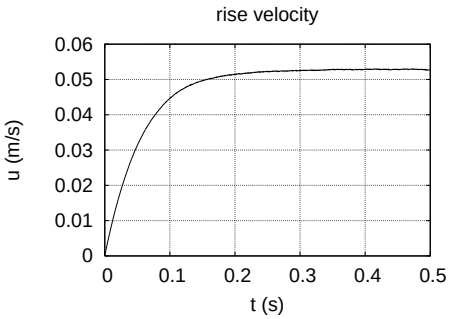

Fig. 9. Rise velocity of a butanol droplet with radius $1\,mm$ as a function of time t.

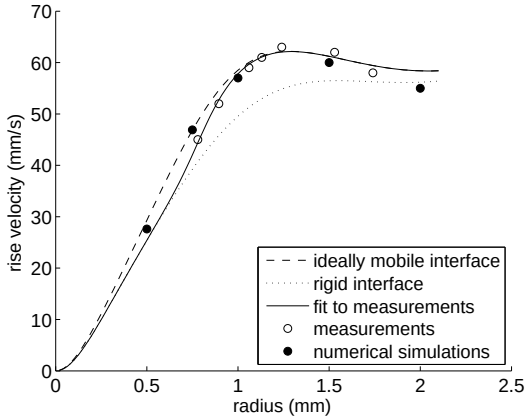

Fig. 10. Terminal rise velocities u_r for different droplet radii r_d. Experimental data (open circles), DROPS simulation results (filled circles) and curve fitted to experimental data (solid line).

Note that $\overline{x}_d'(t) = \overline{\mathbf{u}}_d(t)$ and, due to incompressibility and immiscibility, $\mathrm{vol}(\Omega_1(t)) = \mathrm{vol}(\Omega_1(0))$. For a butanol droplet with radius $1\,mm$ Fig. 9 shows the rise velocity, which is the second coordinate of the average velocity $\overline{\mathbf{u}}_d(t)$. After a certain time the rise velocity becomes almost constant and the droplet reaches a terminal rise velocity denoted by u_r. For the radius $r_d = 1\,mm$ we obtain $u_r = 53\,mm/s$. For technical applications the value of the terminal rise velocity is an important quantity, e. g., to predict the duration of a bubble's residence time inside a column reactor.

We computed the terminal rise velocities u_r of rising butanol droplets for different drop radii r_d. For larger droplets with $r_d \geq 1.5\,mm$ a coarser mesh was used (3 times local refinement instead of 4 times as for the smaller droplets) because of memory limitations. A validation of the simulation results by means of comparison with experimental data is given in [5]. In Fig. 10, which is taken from [5], the terminal rise velocity u_r is plotted versus the droplet radius r_d and a comparison of experimental and simulation results is shown. For a discussion of these results we refer to [5].

The droplet shapes of rising butanol droplets for different radii r_d are shown in Fig. 11. The droplet shape is almost spherical for $r_d = 0.5\,mm$ and becomes more and more flattened for larger radii. The corresponding velocity field $\mathbf{u} - \overline{\mathbf{u}}_d$ (which is the velocity with respect to a reference frame moving with droplet speed $\overline{\mathbf{u}}_d$) is visualized

on a slice in the middle of the domain. Toroidal vortices can be observed inside the droplets. For $r_d = 2\,mm$ we also observe a small vortex structure in the wake of the bubble.

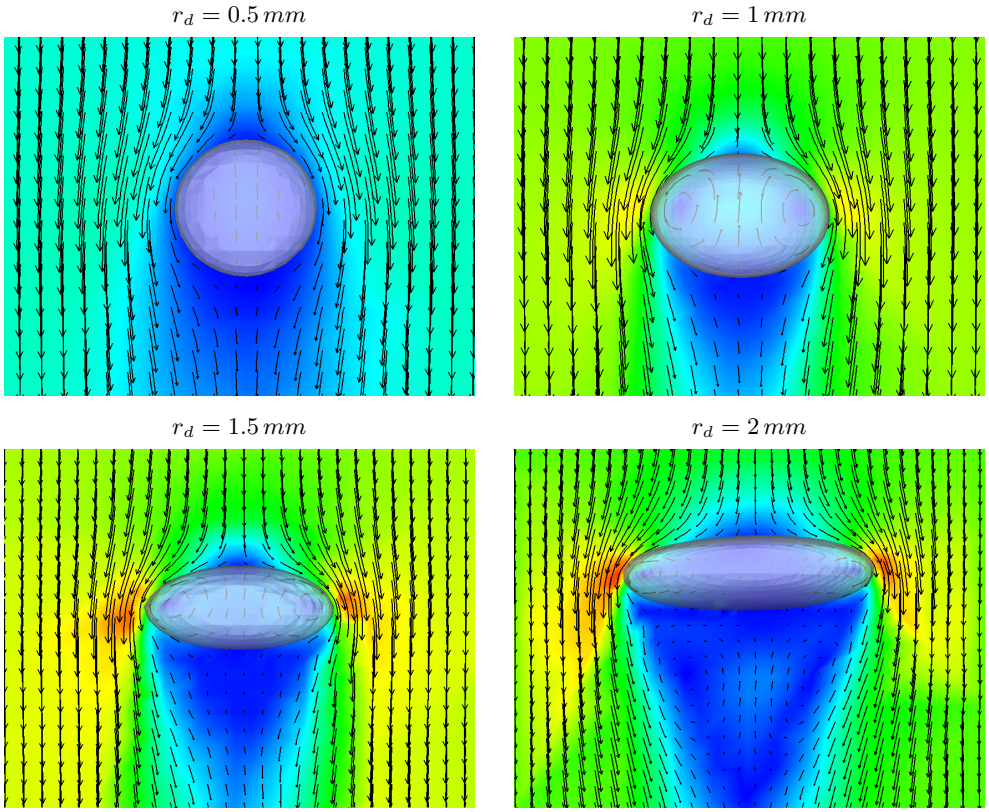

Fig. 11. Shape of n-butanol droplets for different radii r_d and velocity field $\mathbf{u} - \mathbf{u}_d$ visualized on slice.

7.2 Rising toluene droplet with clean interface model

In Section 7.1 we presented simulation results of a rising butanol droplet in water, which is a system with a rather small surface tension coefficient $\tau = 1.63 \cdot 10^{-3}\,N/m$. Now we consider a similar example but with a toluene-water system, where the surface tension coefficient is about 20 times larger. Hence, compared to the butanol-water system the numerical simulation of the fluid dynamics in the toluene-water system is (much) more challenging for the applied numerical methods. The numerical results, taken from [12], illustrate the effect of using the XFEM instead of a standard FEM for discretization of the pressure variable.

Consider a single toluene droplet with an initial spherical shape with radius $r = 10^{-3}\,m$ inside a rectangular tank Ω filled with water, cf. Fig. 6. The experimental setup is chosen as in Section 7.1 except that the material properties of the toluene/water system given in Table 2 are used. Note that the properties of water slightly differ from those in Table 1 which is due to the fact that in the real experi-

ment the water was saturated with toluene at an equilibrium state to avoid any mass transfer between the droplet and the ambient phase.

The same adaptive refinement strategy and discretizations for velocity and level set function as described in Section 7.1 are applied. The pressure is either discretized using the XFEM space $Q_h^{\Gamma_h}$ (cf. Section 6.3) or the standard finite element space Q_h consisting of piecewise linears. Fig. 12 shows the initial shape of the droplet and the droplet shapes after 10 time steps for both cases.

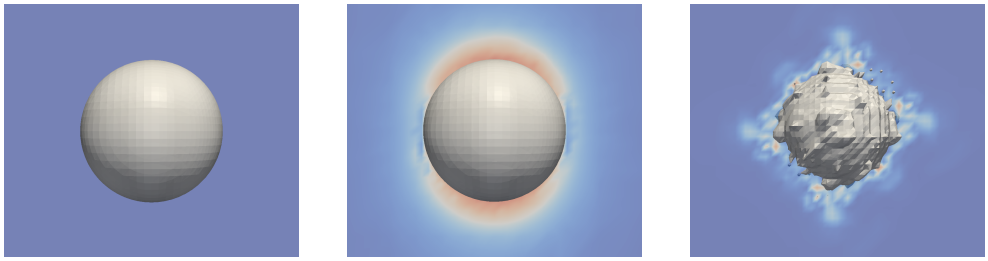

Fig. 12. Initial droplet shape (left) and after 10 time steps for the XFEM case (middle) and the standard FEM case (right).

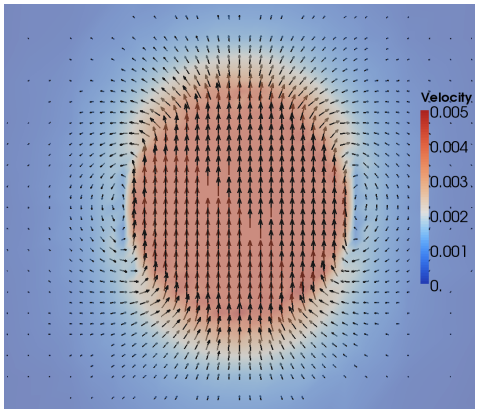

Fig. 13. Velocity field at interface for the XFEM case.

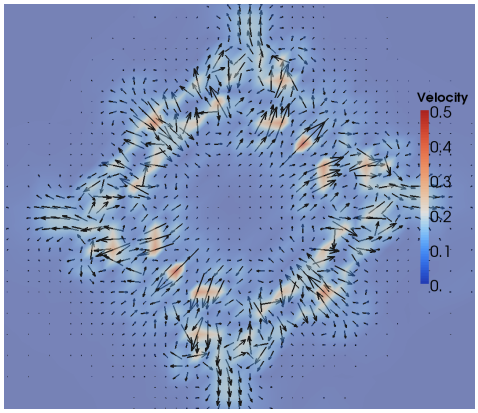

Fig. 14. Velocity field at interface for the standard FEM case.

While the interface is smooth using the extended pressure finite element space, it shows many "spikes" in the case of the standard pressure space. These spikes are of course non-physical and only caused by numerical oscillations at the interface, so-called *spurious velocities*, which are shown in Fig. 14. The velocity field for the XFEM case is smooth showing the characteristic vortices, cf. Fig. 13. Note that the scaling of the color coding in both figures is very different, with a maximum velocity of $5 \cdot 10^{-3}\, m$ for the extended pressure space compared to $5 \cdot 10^{-1}\, m$ for the standard pressure space. These results clearly show, that for this realistic two-phase flow example the standard pressure space Q_h is not suitable, whereas the extended pressure space $Q_h^{\Gamma_h}$ yields satisfactory results.

7.3 Spherical droplet in Poisseuille flow with Boussinesq-Scriven interface stress model

In this section we consider the one-fluid model described in Section 4 with the Boussinesq-Scriven interface tensor as in (7). The result is taken from [18]. In that report the one-fluid Navier-Stokes model with Boussinesq-Scriven viscous interface forces is compared with a recent theoretical study in [20]. In the latter paper one considers an isolated spherical droplet in a Stokes Poisseuille flow with a jump in the hydrodynamic stress at the interface determined by surface viscous forces according to the Boussinesq-Scriven law. Analytical results for the so-called *migration velocity* are derived.

We give a more precise definition of the model used in [20]. The stationary bulk phase Ω_1 is a ball with radius r which has its center on the x-axis, and $\Omega_2 = \mathbb{R}^3 \setminus \Omega_1$. In both phases creeping flow conditions are assumed, i. e.,

$$\begin{cases} -\mu_i \Delta \mathbf{u} + \nabla p = 0 \\ \operatorname{div} \mathbf{u} = 0 \end{cases} \qquad \text{in } \Omega_i, \quad i = 1, 2. \tag{43}$$

Instead of a boundary condition the far field condition

$$\mathbf{u}(\mathbf{x}) \to \mathbf{u}^{\mathrm{P}}(\mathbf{x}) \quad \text{for } \|\mathbf{x}\| \to \infty \tag{44}$$

is assumed with $\mathbf{u}^{\mathrm{P}}$ given by a Poisseuille flow profile

$$\mathbf{u}^{\mathrm{P}}(y) = U_{center}(1 - \alpha y^2)\, \mathbf{e}_x, \tag{45}$$

with given constants $U_{center} > 0$, $\alpha > 0$. At the interface Γ both kinematic and dynamic boundary conditions are imposed. Define the (droplet) mean velocity $\mathbf{U}_T := \frac{1}{|\Omega_1|} \int_{\Omega_1} \mathbf{u}\, d\mathbf{x}$. The interface conditions are given by

$$[\mathbf{u}]_\Gamma = 0 \qquad \text{on } \Gamma, \tag{46a}$$

$$\mathbf{u} \cdot \mathbf{n}_\Gamma = \mathbf{U}_T \cdot \mathbf{n}_\Gamma \qquad \text{on } \Gamma, \tag{46b}$$

$$[\mathbf{P}\boldsymbol{\sigma}\mathbf{n}]_\Gamma = \mathbf{P} \operatorname{div}_\Gamma \boldsymbol{\sigma}_\Gamma \qquad \text{on } \Gamma, \tag{46c}$$

with $\boldsymbol{\sigma}$ the Newtonian bulk stress tensor and $\boldsymbol{\sigma}_\Gamma$ the Boussinesq-Scriven interface stress tensor. Note that (46b) enforces a normal velocity consistent with a rigid body translation. To obtain a well-posed problem only the *tangential* stress balance condition (46c) is imposed. There are no external forces (i. e., a neutrally buoyant droplet), but the interface stress tensor $\boldsymbol{\sigma}_\Gamma$ allows surface viscous forces.

The difference between the droplet mean velocity $\mathbf{U}_T$ and the unperturbed Poisseuille flow on the x-axis $\mathbf{u}^{\mathrm{P}}(0)$ is called the *migration velocity*:

$$\mathbf{U}_{mig} := \mathbf{U}_T - \mathbf{u}^{\mathrm{P}}(0). \tag{47}$$

In [20] explicit formulas for $\mathbf{U}_{mig}$ are derived. The analysis relies on a representation of $\mathbf{u}$ and $\mathbf{u}^{\mathrm{P}}$ in the basis of spherical harmonics. In the analysis it is essential that the droplet is *spherical*. The following result is from [20], with the dimensionless dilatational Boussinesq number $Bo^d := \frac{\lambda_\Gamma}{\mu_2 r}$ and the viscosity ratio $\xi := \frac{\mu_1}{\mu_2}$:

$$\mathbf{U}_{mig} = -\frac{2Bo^d + 3\xi}{3(2 + 2Bo^d + 3\xi)} \alpha r^2\, \mathbf{e}_x. \tag{48}$$

Note that there is a monotonic dependence of $\mathbf{U}_{mig}$ on Bo^d and *no dependence* on the dimensionless shear Boussinesq number $Bo^s := \frac{\mu_\Gamma}{\mu_2 r}$.

In [18] it is studied, whether a Navier-Stokes two-phase flow that is "close to" the Stokes regime (low Reynolds number) and with a droplet that remains almost spherical (small capillary number and small Weber number) leads to a similar relation between dilatational/shear Boussinesq number and migration velocity. As an example, a result is given in Fig. 16. In the Navier-Stokes simulation the following data are used. The computational domain is given by $\Omega = [0, 0.3] \times [-0.05, 0.05] \times [-0.15, 0.15]\ m^3$. On the z-boundaries we use periodic boundary conditions. On the y-boundaries we take Dirichlet no-slip conditions ($\mathbf{u} = 0$). On the x-inflow boundary we prescribe a Poisseuille profile as in (45) with $U_{center} = 0.0125\, m/s$, $\alpha = 5\,(ms)^{-}1$. On the x-outflow boundary we impose the zero stress condition $\boldsymbol{\sigma}\mathbf{n} = 0$. A sketch of the cross section of Ω at $z = 0$ is given in Fig. 15.

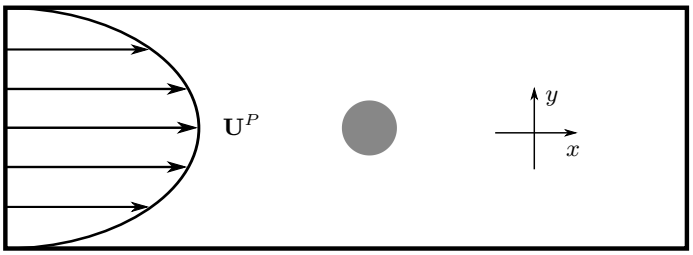

Fig. 15. Cross section of the domain used in numerical simulations.

The initial phase-1 domain $\Omega_1(0)$ is a sphere with radius 0.0125 m with center located at the center of Ω. The initial velocity $\mathbf{u}(0)$ is obtained by solving the corresponding stationary Stokes problem. Furthermore, in the one-fluid model with Boussinesq-Scriven interface stresses we use the parameters $\rho_1 = \rho_2 = 1$, $\mu_1 = 2$, $\mu_2 = 1$, $\tau = 0.1$, $\mu_\Gamma = 0$ and we take different values for the dilatational Boussinesq number $Bo^d \in \{1, 2, 5, 10, 20, 50, 100\}$. For this case ($\xi = 2,\ \alpha = 5,\ r = 0.0125$) the theoretical relation (48) and results for the migration velocity in the Navier-Stokes model are shown in Fig. 16.

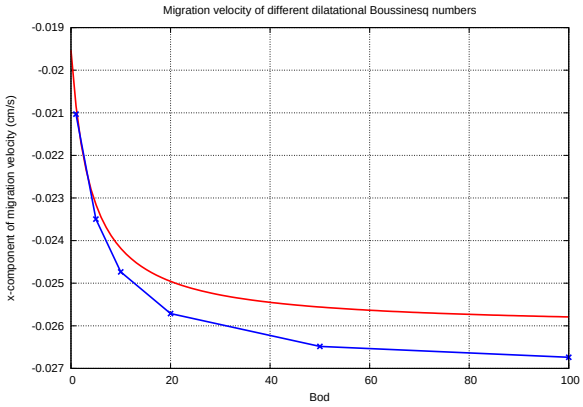

Fig. 16. Migration velocities: comparison between theoretical Poisseuille Stokes flow (upper curve) and Navier-Stokes model (lower curve).

As far as we know there are no other papers in which numerical simulation results of two-phase flows based on the Navier-Stokes one-fluid model with Boussinesq-Scriven interface stresses are presented.

References

1. S. Aland, J. Lowengrub, and A. Voigt. A continuum model of colloid stabilized interfaces. *Physics of Fluids*, 23:062103, 2011.
2. D. Anderson, G. McFadden, and A. Wheeler. Diffusive-interface methods in fluid mechanics. *Annu. Rev. Fluid Mech.*, 30:139–165, 1998.
3. R. Aris. *Vectors, tensors, and the basic equations of fluid mechanics*. Dover Publications, 1989.
4. T. Belytschko, N. Moës, S. Usui, and C. Parimi. Arbitrary discontinuities in finite elements. *Int. J. Numer. Meth. Engrg.*, 50:993–1013, 2001.
5. E. Bertakis, S. Groß, J. Grande, O. Fortmeier, A. Reusken, and A. Pfennig. Validated simulation of droplet sedimentation with finite-element and level-set methods. *Chemical Eng. Science*, 65:2037–2051, 2010.
6. DROPS package for simulation of two-phase flows. `http://www.igpm.rwth-aachen.de/DROPS/`.
7. G. Dziuk. Finite elements for the Beltrami operator on arbitrary surfaces. In S. Hildebrandt and R. Leis, editors, *Partial differential equations and calculus of variations*, volume 1357 of *Lecture Notes in Mathematics*, pages 142–155. Springer, 1988.
8. G. Dziuk and C. Elliott. Finite elements on evolving surfaces. *IMA J. Numer. Anal.*, 27:262–292, 2007.
9. T. Fries and T. Belytschko. The generalized/extended finite element method: An overview of the method and its applications. *Int. J. Numer. Meth. Engrg.*, 84:253–304, 2010.
10. T. Fries and A. Zilian. The extended finite element method. *Int. J. Numer. Meth. Engrg.*, 2011. special issue.
11. S. Groß and A. Reusken. Finite element discretization error analysis of a surface tension force in two-phase incompressible flows. *SIAM J. Numer. Anal.*, 45(4):1679–1700, 2007.
12. S. Gross and A. Reusken. *Numerical Methods for Two-phase Incompressible Flows*. Springer, Heidelberg, 2011.
13. C. Lehrenfeld and A. Reusken. Analysis of a DG-XFEM discretization for a class of two-phase mass transport problems. Technical Report 340, IGPM, RWTH-Aachen, 2012.
14. N. Moës, J. Dolbow, and T. Belytschko. A finite element method for crack growth without remeshing. *Int. J. Numer. Meth. Engrg.*, 46:131–150, 1999.
15. M. Olshanskii, A. Reusken, and J. Grande. An Eulerian finite element method for elliptic equations on moving surfaces. *SIAM J. Numer. Anal.*, 47:3339–3358, 2009.
16. S. Osher and R. Fedkiw. *Level Set Methods and Dynamic Implicit Surfaces*. Applied Mathematical Sciences,Vol. 153. Springer, Berlin, Heidelberg, New York, 2003.
17. L. Rayleigh. On the theory of surface forces - II. compressible fluids. *Phil. Mag.*, 30:209–220, 1892.
18. A. Reusken and Y. Zhang. Numerical simulation of incompressible two-phase flows with a Boussinesq-Scriven interface stress. Technical report, IGPM, RWTH-Aachen, 2012.
19. L. Sagis. Dynamic properties of interfaces in soft matter: experiments and theory. *Rev. Mod. Phys.*, 83(4):1367, 2011.
20. J. T. Schwalbe, F. R. Phelan, Jr., P. M. Vlahovska, and S. D. Hudson. Interfacial effects on droplet dynamics in Poiseuille flow. *Soft Matter*, 7:7797–7804, 2011.
21. J. Sethian. *Level Set Methods and Fast Marching Methods*. Cambridge University Press, 1999.
22. J. Slattery, L. Sagis, and E.-S. Oh. *Interfacial Transport Phenomena*. Springer, New York, second edition, 2007.

23. K. Teigen, X. Li, J. Lowengrub, F. Wang, and A. Voigt. A diffusion-interface approach for modelling transport, diffusion and adsorption/desorption of material quantities on a deformable interface. *Comm. Math. Sci.*, 7:1009–1037, 2009.
24. K. Teigen, P. Song, J. Lowengrub, and A. Voigt. A diffusive-interface method for two-phase flows with soluble surfactants. Technical report, Department of Mathematics, TU-Dresden, 2010.
25. V. Thomee. *Galerkin Finite Element Methods for Parabolic Problems*. Springer, Berlin, 1997.
26. G. Tryggvason, R. Scardovelli, and S. Zaleski. *Direct Numerical Simulations of Gas-Liquid Multiphase Flows*. Cambridge University Press, Cambridge, 2011.
27. J. Van der Waals. The thermodynamic theory of capillarity under the hypothesis of a continuous density variation. *J. Stat. Phys.*, 20:197–244, 1893.